A hybrid coupled wave-number integration approach to range-dependent seismoacoustic modeling

Joo Thiam Goh and Henrik Schmidt
Department of Ocean Engineering, Massachusetts Institute of Technology, Cambridge, Massachusetts 02139

(Received 30 January 1996; accepted for publication 24 April 1996)

Recently, a *spectral super-element* approach was developed for acoustic modeling in fluid waveguides [H. Schmidt, W. Seong, and J. T. Goh, J. Acoust. Soc. Am. **98**, 465–472 (1995)]. The approach uses a hybridization of finite elements, boundary integrals, and wave-number integration to solve the Helmholtz equation in a range-dependent ocean environment. It provides accurate, full two-way solutions to the wave equation, using either a full, global multiple scattering solution technique, or an efficient single-scatter, marching solution. This paper extends that work to mixed fluid-elastic stratifications. SAFARI is used as the basic computational engine for generating the Green's function in an ocean with arbitrary fluid-elastic stratifications. The hybrid model therefore directly provides the spectral decomposition of the wave field in terms of modal components, head waves as well as seismic interface waves. Extensive numerical experiments have shown that the method gives accurate results particularly in the forward scatter direction. For comparisons, we have used a finite element parabolic equation model, a boundary-element code, as well as the recently developed virtual source algorithm. © *1996 Acoustical Society of America.*

PACS numbers: 42.30.Bp, 43.30.Dr, 43.30.Gv [MBP]

INTRODUCTION

In recent years, there has been a shift from deep ocean acoustics to the littoral or shallow water acoustics and with it, the recognition that range dependence and the elasticity of the seabed play an important role in the overall propagation, particularly in the low frequency regime. The shallow water environment is an extremely complicated waveguide bounded above by a rough sea surface and below by an inhomogeneous, multi-layered elastic seabed. Further, the acoustic properties of the water column are dependent on temperature, pressure and salinity, giving rise to a significant spatial and temporal variation. The elastic seabed added another degree of complication and it is only recently that modelers have been able to account for its effect to some degree. The excitation and propagation behaviors of seismic interface modes, inhomogeneous waves, and both headwave and multiply reflected wave interference are all important phenomena and the energy carried by seismic waves is not negligible compared to the water-borne field.

For range-independent seismoacoustic propagation modeling, SAFARI[1] is in widespread use for providing exact reference solutions. Since SAFARI is based on integral transforms of the wave equation, it is not directly applicable to range-dependent problems. Lu and Felsen[2] derived an adiabatic transformation of the wave-number integrals for weakly range-dependent problems. However, the method works well only for cases where the wave field is largely dominated by *discrete modes*.[3] Its extension to the elastic case is also non-trivial. There have been attempts to use the more general discrete approaches such as the finite difference methods (FDM),[4] and the finite element methods (FEM).[5] However, since these methods rely on spatial and temporal discretizations which are small compared to the wavelengths, they are normally restricted to modeling short range propagation and scattering.

The *parabolic equation* (PE) algorithm today is without doubt the most popular approach to modeling range-dependent ocean waveguides. However, in trying to extend the PE theory to elastic media, two main problems arise. First, the field is described by a vector (displacement) rather than a scalar. Second, two different wave speeds exist in a solid and in a heterogeneous media or at boundaries, we have continuous conversion from one wave type to another. Furthermore, elastic bottoms support a wide spectrum of propagation angles. Therefore, even though several PE models have been proposed for wave propagation in elastic media,[6–12] only a few of these models were implemented. Notable implementations include those of Wetton and Brooke[10] and Collins.[11,12] Thus, for the most part, the parabolic theories for elastic waves have not been adequately tested numerically, particularly in two-way formulations. In addition to being limited to weak range dependence, a major drawback of the PE as well as the discrete methods is the fact that the solutions are not as easily interpreted physically. Thus, the modal structure of the field can only be determined through post-processing.[13]

In this paper, we extend the work in Ref. 14 to arbitrary fluid-elastic stratifications. The proposed modeling approach can provide full two-way global solution but is currently implemented using the more efficient single-scatter formulation. We present both forward and backscatter numerical solutions to a series of benchmark problems.

I. THE SPECTRAL SUPER-ELEMENT APPROACH

A. Stratified super-elements

In the *spectral super-element* approach, the environment is first divided into a series of range-independent *sectors* or

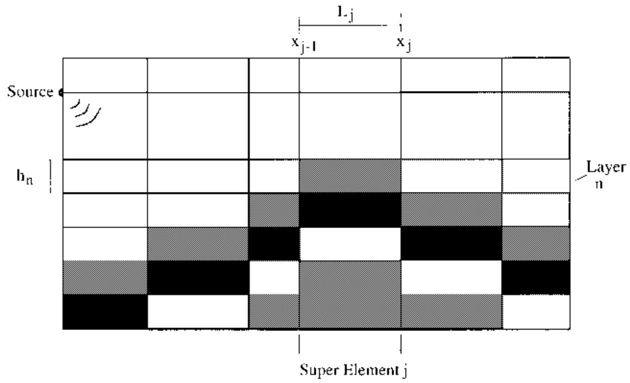

FIG. 1. Super-element discretization of range-dependent ocean waveguides.

super-elements, separated by vertical boundaries or *cuts*, as illustrated in Fig. 1. Within each sector, the ocean environment is horizontally stratified and we will allow for arbitrary fluid-elastic stratifications.

In deriving the spectral-element equations we will assume the acoustic field to be plane. Thus, in order to account for cylindrical spreading in axisymmetric scenarios, the spreading factor is applied explicitly to the resulting field. The validity of this approach is described in the appendix of Ref. 14.

The equations of motion for a homogeneous isotropic elastic solid in plane strain are given by[15,16]

$$(\lambda+2\mu)\nabla\nabla\cdot\mathbf{u}-\mu\nabla\times\nabla\times\mathbf{u}+\rho\mathbf{f}=\rho\frac{\partial^2\mathbf{u}}{\partial t^2}, \tag{1}$$

where λ and μ are the Lamè constants, ρ is the density, $\mathbf{u}=(u,w)$ is the displacement vector, and $\mathbf{f}$ is the body force per unit mass of material. We write the displacement vector in terms of two scalar potential fields, ϕ and ψ, i.e.,

$$\mathbf{u}=\nabla\phi+\nabla\times(0,\psi,0), \tag{2}$$

where the first and second term represents the dilatational and rotational part of the solution respectively. These potentials are solutions of the scalar wave equations

$$\nabla^2\phi=\frac{1}{c_p^2}\frac{\partial^2\phi}{\partial t^2}, \quad \nabla^2\psi=\frac{1}{c_s^2}\frac{\partial^2\psi}{\partial t^2}, \tag{3}$$

where c_p and c_s are the compressional and shear wave speeds respectively, and are given by

$$c_p^2=\frac{\lambda+2\mu}{\rho}, \quad c_s^2=\frac{\mu}{\rho}.$$

Assuming an $\exp(i\omega t)$ harmonic time dependence (suppressed henceforth), the potentials then also satisfy the following Helmholtz equations:

$$(\nabla^2+h^2)\phi=0, \quad (\nabla^2+\kappa^2)\psi=0,$$

where $h=\omega/c_p$ and $\kappa=\omega/c_s$ denote the wave numbers for the compressional and shear waves, respectively.

The field in each sector is now expressed as a superposition of the field produced in the stratified element in the absence of the vertical boundaries, $\mathbf{u}^*$, the field arising from the left boundary $\mathbf{u}^-$, and the field arising from the right boundary, $\mathbf{u}^+$,

$$\mathbf{u}(x,z)=\mathbf{u}^*(x,z)+\mathbf{u}^-(x,z)+\mathbf{u}^+(x,z), \tag{4}$$

where $\mathbf{u}$ is taken to denote contributions from the potential ϕ and in the case of an elastic stratification, also includes contributions from ψ.

The wave fields are determined using an *indirect* boundary integral method,[14] based on Green's theorem for the semi-infinite virtual element obtained by eliminating the other vertical boundary and letting the element continue to infinity,

$$\mathbf{u}_i^{\pm}(\mathbf{r})=\int_{S^{\pm}}[G_{ji}(\mathbf{r};\mathbf{r}^{\pm})t_j(\mathbf{r};\mathbf{n}^{\pm}) -H_{ji}(\mathbf{r};\mathbf{r}^{\pm};\mathbf{n}^{\pm})u_j(\mathbf{r})]dS^{\pm}. \tag{5}$$

Here $u_j(\mathbf{r})$ and $t_j(\mathbf{r};\mathbf{n}^{\pm})$ are the r_j components of the displacements and tractions on the boundary of the semi-infinite elements $S^{\pm}$. $G_{ji}(\mathbf{r},\mathbf{r}^{\pm})$ and $H_{ji}(\mathbf{r},\mathbf{r}^{\pm};\mathbf{n}^{\pm})$ are the jth components of the displacement and traction of the Green's functions at the point $\mathbf{r}$ on the surface $S^{\pm}$ with outgoing normal $\mathbf{n}^{\pm}$, due to a unit force applied in the ith direction at a point $\mathbf{r}^{\pm}$.

Note here, that the super-elements always have finite depth. Thus, in the presence of a lower half-space, the lower boundary of the super-element is chosen deep enough into the half-space to ensure that the field satisfies the radiation condition along the horizontal boundary, in which case the associated surface integral contribution vanishes.

To solve the integral equation in Eq. (5), we introduce both symmetric and antisymmetric panel sources at the boundary. A displacement formulation in combination with the Galerkin approach is then used to reduce the integral equation into a system of linear equations, the unknowns of which are the source strengths for the panel sources. Once these unknown source strengths are determined, the wavefield in each sector can be determined efficiently using fast field program (FFP) techniques. As in the direct global matrix (DGM) method, we express the field in each layer as a superposition of the field produced by the panel source within the layer in the absence of boundaries, referred to as the *direct* panel contribution $\hat{\mathbf{u}}$, and an unknown field $\overline{\mathbf{u}}$ which is necessary to satisfy the boundary conditions at the layer interfaces

$$\mathbf{u}=\hat{\mathbf{u}}+\overline{\mathbf{u}}. \tag{6}$$

The latter field must satisfy the homogeneous equations of motion and is referred to as the *homogeneous* solution. In other words, they are the source-free waves that must be added to the direct panel contributions to satisfy the boundary conditions. The homogeneous field is governed by Eq. (1) with the body force term $\mathbf{f}$ equal to zero.

B. Field expansion

The boundary conditions to be satisfied between the super-elements, together with Eq. (5), now provides an integral equation for the field $\mathbf{u}^{\pm}$ on the vertical boundaries of the super-element, the numerical solution of which requires some kind of discretization. For fluid super-elements, the boundary conditions are the continuity of pressure and particle displacement, i.e. at the vertical boundary j separating super-elements j and $j+1$,

$$\begin{Bmatrix} u(x_j,z) \\ p(x_j,z) \end{Bmatrix}^j = \begin{Bmatrix} u(x_j,z) \\ p(x_j,z) \end{Bmatrix}^{j+1}, \tag{7}$$

and for elastic super-elements, the boundary conditions are the continuity of stresses and displacements, i.e.,

$$\begin{Bmatrix} u(x_j,z) \\ w(x_j,z) \\ \sigma_{xx}(x_j,z) \\ \sigma_{xz}(x_j,z) \end{Bmatrix}^j = \begin{Bmatrix} u(x_j,z) \\ w(x_j,z) \\ \sigma_{xx}(x_j,z) \\ \sigma_{xz}(x_j,z) \end{Bmatrix}^{j+1}. \tag{8}$$

A superscript is used to identify the super-element here and in the following. Since the field within each layer in the stratification is a smooth function of depth, we here choose a *Galerkin boundary element* approach.[17] In the Galerkin approach, the continuity of the field across the vertical boundaries is expressed in the *weak form*

$$\int_0^{t_\ell} \mathbf{u}^j(x_j,z)[\mathbf{u}^{j+1}(x_j,z)-\mathbf{u}^j(x_j,z)]dz=0, \tag{9}$$

and similarly for the stresses. The displacements and stresses are now expressed as expansions in terms of a set of basis functions. By choosing an orthogonal set of expansion functions Eq. (9) requires the expansion coefficients in the two neighboring sectors to be identical. Here we choose an orthonormal set of Legendre polynomials, normalized within each layer ℓ:

$$\begin{Bmatrix} u(x,z) \\ w(x,z) \\ \sigma_{xx}(x,z)/\mu \\ \sigma_{xz}(x,z)/\mu \end{Bmatrix}^j = \frac{2\pi}{t_\ell}\sum_{m=1}^{\infty} \begin{Bmatrix} U_{\ell m}(x) \\ W_{\ell m}(x) \\ T_{\ell m}(x) \\ S_{\ell m}(x) \end{Bmatrix}^j P_{m-1}(\overline{z}), \tag{10}$$

where m is the order of expansion, P_m is the Legendre function, and t_ℓ is the thickness of layer ℓ. The argument to the Legendre polynomial is the normalized, local depth coordinate

$$\overline{z} = \frac{z-t_\ell/2}{t_\ell/2}. \tag{11}$$

The expansion coefficients $U_{\ell m}(x)$ through $S_{\ell m}(x)$ are functions of $U_{\ell m}(0)$ and $W_{\ell m}(0)$, the unknown panel source strengths of the symmetric and antisymmetric source, respectively. In effect, they are like the Green's functions for the panel sources. As outlined earlier, we decompose these Green's functions into two components: one corresponding to the direct field due to the panel source in the layer, the other corresponding to the reflections from the layer interfaces. We can then write the expansion coefficient $U_{\ell m}(x)$ as

$$U_{\ell m}(x) = \hat{U}_{\ell m}(x) + \overline{U_{\ell m}}(x), \tag{12}$$

where $\hat{U}_{\ell m}(x)$ and $\overline{U_{\ell m}}(x)$ denote the direct and homogeneous contributions, respectively. The other coefficients can also be written in a similar manner. These expansion coefficients are used in the Galerkin scheme when solving the boundary integral equation. We first derive vertical wave-number representations and subsequently these are transformed into horizontal wave-number representations suitable for the DGM method. These latter forms are also useful for efficient computation of the resultant field.

C. Direct panel source contribution

We start by defining the potentials for the panel sources. The compressional and shear displacement potentials which satisfy the Helmholtz equation and the radiation condition can be written in terms of a vertical wave-number spectral representation as

$$\begin{aligned} \phi_\ell(x,z) &= \int_{-\infty}^{\infty} A_\ell(\eta) e^{-x\gamma} e^{-i\eta(z-t_\ell/2)} d\eta, \\ \psi_\ell(x,z) &= \int_{-\infty}^{\infty} B_\ell(\eta) e^{-x\delta} e^{-i\eta(z-t_\ell/2)} d\eta, \end{aligned} \tag{13}$$

where η, $i\gamma = i\sqrt{\eta^2-h^2}$ and $i\delta = i\sqrt{\eta^2-\kappa^2}$ are the vertical and horizontal wave numbers, respectively. The quantities $A_\ell(\eta)$ and $B_\ell(\eta)$ are the source spectrums to be determined from boundary conditions at the vertical interface.

1. The symmetric problem

The symmetric problem is characterized by two conditions at the discontinuity $(x=0)$,

$$\sigma_{xz}(0,z)/\mu = \frac{\partial u}{\partial z} + \frac{\partial w}{\partial x} = 0, \tag{14}$$

$$\begin{aligned} u(0,z) &= \frac{\partial \phi}{\partial x} - \frac{\partial \psi}{\partial z} \\ &= \begin{cases} \dfrac{2\pi}{t_\ell}\displaystyle\sum_{m=1}^{\infty} U_{\ell m}(0) P_{m-1}(\overline{z}), & 0 \leq z \leq t_\ell \\ 0, & \text{otherwise.} \end{cases} \end{aligned} \tag{15}$$

Substitution of Eq. (13) into Eq. (15) yields a relationship between $U_{\ell m}(0)$ and $A_\ell(\eta)$ and subsequently Eq. (15) becomes

$$\begin{aligned} u(0,z) &= \int_{-\infty}^{\infty} \frac{\gamma\kappa^2}{\varphi} A_\ell^{(1)}(\eta) e^{i\eta t_\ell/2} e^{-i\eta z} d\eta, \\ &= \frac{2\pi}{t_\ell}\sum_{m=1}^{\infty} U_{\ell m}(0) P_{m-1}(\overline{z}), \end{aligned} \tag{16}$$

where $\varphi = 2\eta^2 - \kappa^2$. We define the Fourier transform pair as

$$\begin{aligned} f(z) &= \int_{-\infty}^{\infty} g(\eta) e^{-i\eta z} d\eta, \\ g(\eta) &= \frac{1}{2\pi}\int_{-\infty}^{\infty} f(z) e^{i\eta z} dz, \end{aligned} \tag{17}$$

and taking the forward transform with respect to z of Eq. (16), we obtain

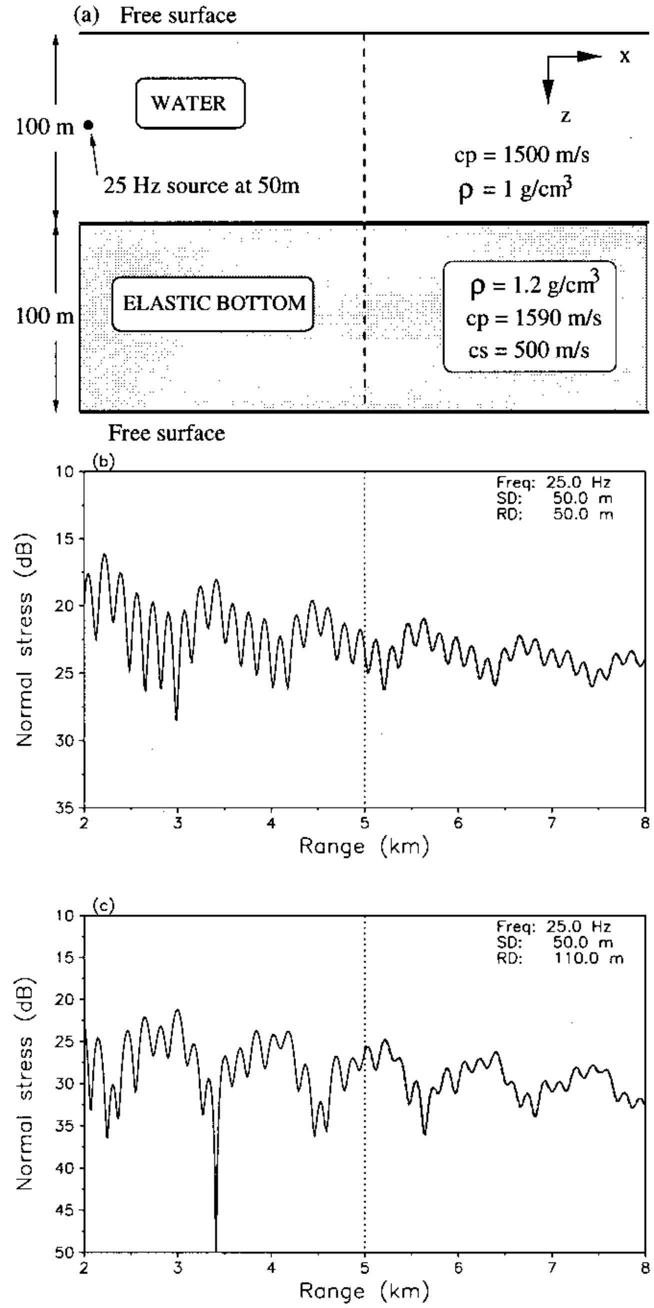

FIG. 2. Modified NORDA 3A test case (Ex. A). (a) Test configuration, (b) receiver at 50 m, (c) receiver at 110 m. Solid : SAFARI, dashed: spectral super-element.

$$\frac{\gamma\kappa^2}{\varphi} A_\ell^{(1)}(\eta) e^{i\eta t_\ell/2} = \frac{1}{t_\ell}\sum_{m=1}^{\infty} U_{\ell m}(0)\int_0^{t_\ell} P_{m-1}(\overline{z}) e^{i\eta z}\, dz. \tag{18}$$

Making use of the relation,[18]

$$\int_0^{t_\ell} P_{m-1}(\overline{z}) e^{i\eta z}\, dz = t_\ell e^{i\eta(t_\ell/2)} i^{m-1} j_{m-1}\left(\frac{t_\ell \eta}{2}\right), \tag{19}$$

where j_{m-1} is the spherical Bessel function, we obtain for the symmetric part of the source spectrum $A_\ell(\eta)$,

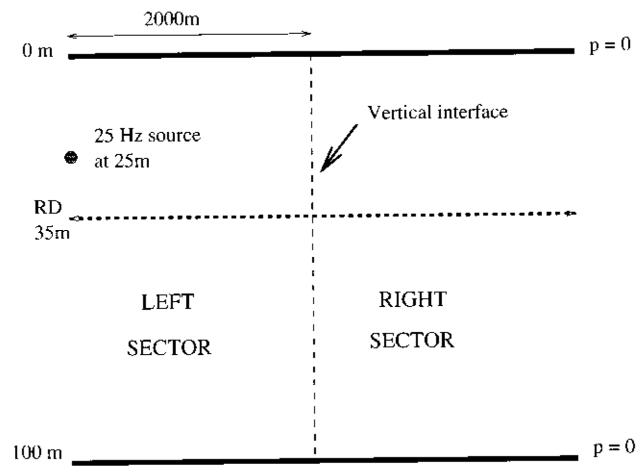

FIG. 3. Ex. B : Configuration for the single layer benchmarks.

$$A_\ell^{(1)}(\eta) = \frac{\varphi}{\kappa^2\gamma}\sum_{m=1}^{\infty} U_{\ell m}(0) i^{m-1} j_{m-1}\left(\frac{t_\ell \eta}{2}\right). \tag{20}$$

Substitution of the above into Eq. (14) yields

$$B_\ell^{(1)}(\eta) = -\frac{2i\eta}{\kappa^2}\sum_{m=1}^{\infty} U_{\ell m}(0) i^{m-1} j_{m-1}\left(\frac{t_\ell \eta}{2}\right). \tag{21}$$

2. The antisymmetric problem

The antisymmetric problem is similarly characterized by two conditions at the discontinuity,

$$\sigma_{xx}(0,z)/\mu = \left(\frac{\lambda + 2\mu}{\mu}\right)\frac{\partial u}{\partial x} + \frac{\lambda}{\mu}\frac{\partial w}{\partial z} = 0, \tag{22}$$

$$w(0,z) = \frac{\partial\phi}{\partial z} + \frac{\partial\psi}{\partial x}$$

$$= \begin{cases} \dfrac{2\pi}{t_\ell}\displaystyle\sum_{m=1}^{\infty} W_{\ell m}(0) P_{m-1}(\overline{z}), & 0 \leqslant z \leqslant t_\ell, \\ 0, & \text{otherwise.} \end{cases} \tag{23}$$

After some algebra we obtain the antisymmetric part of the source spectrum as

$$A_\ell^{(2)}(\eta) = \frac{2i\eta}{\kappa^2}\sum_{m=1}^{\infty} W_{\ell m}(0) i^{m-1} j_{m-1}\left(\frac{t_\ell \eta}{2}\right), \tag{24}$$

$$B_\ell^{(2)}(\eta) = \frac{\varphi}{\kappa^2\delta}\sum_{m=1}^{\infty} W_{\ell m}(0) i^{m-1} j_{m-1}\left(\frac{t_\ell \eta}{2}\right). \tag{25}$$

3. Series representations for the direct panel field

The unknown panel source strengths $U_{\ell m}(0)$ and $W_{\ell m}(0)$ are now determined through matching the relevant boundary conditions at the vertical cut. We do this by the Galerkin boundary element approach which simply requires that the expansion coefficients in the two neighboring sectors be identical. These expansion coefficients can be straightforwardly extracted from the potential representations above by using the orthogonality relation for the Legendre polynomi-

TABLE I. Parameters for the series of two-sector canonical test problems. Wave speeds are given in m/s, densities in g/cm^3, and attenuation in dB/λ.

	Parameters	B1	B2	B3	B4
		Benchmark			
Left sector	ρ	1.0	1.5	1.5	1.5
	c_p	1500	1700	1700	1700
	c_s	0	700	700	700
	α_p	0.2	0.2	0.2	0.2
	α_s	0	0.5	0.5	0.5
Right sector	ρ	1.5	1.0	1.5	1.5
	c_p	1700	1500	1800	3000
	c_s	700	0	900	1700
	α_p	0.2	0.2	0.2	0.2
	α_s	0.5	0	0.5	0.5

als. In practice, we need to truncate the infinite series expansions at a sufficiently high order. Since the Legendre polynomials represent the vertical variation in the field, one can obtain the truncation limit from an estimate of the number of normal modes.

Let us consider the coefficient $\hat{U}_{\ell k}(x)$,

$$u_{\ell}(x,z)=\frac{2\pi}{t_{\ell}}\sum_{k=1}^{\infty}\hat{U}_{\ell k}(x)P_{k-1}(\overline{z}). \tag{26}$$

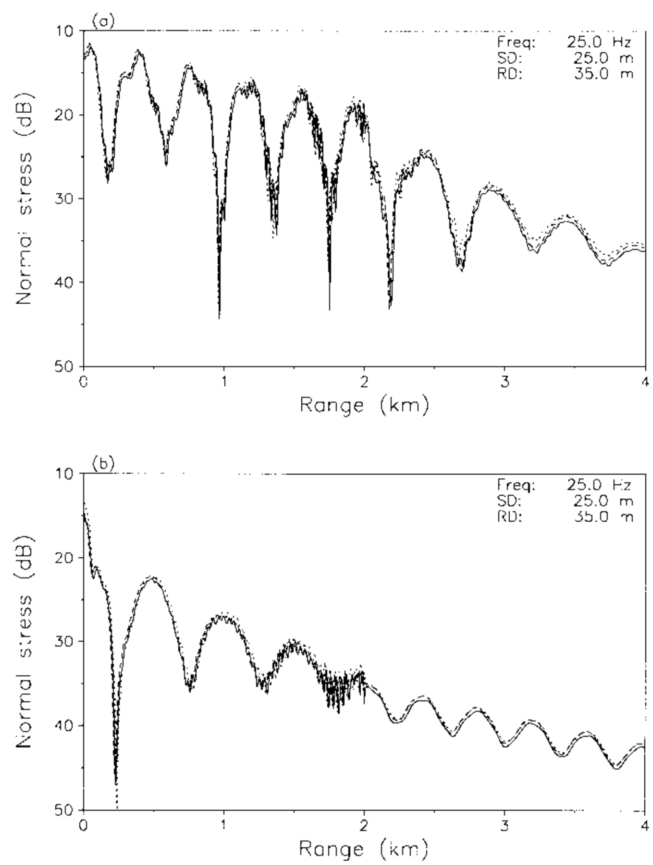

FIG. 4. Solutions to the single layer benchmarks. (a) case B1, (b) case B2, solid: BEM, dashed : VISA, dotted: spectral super-element.

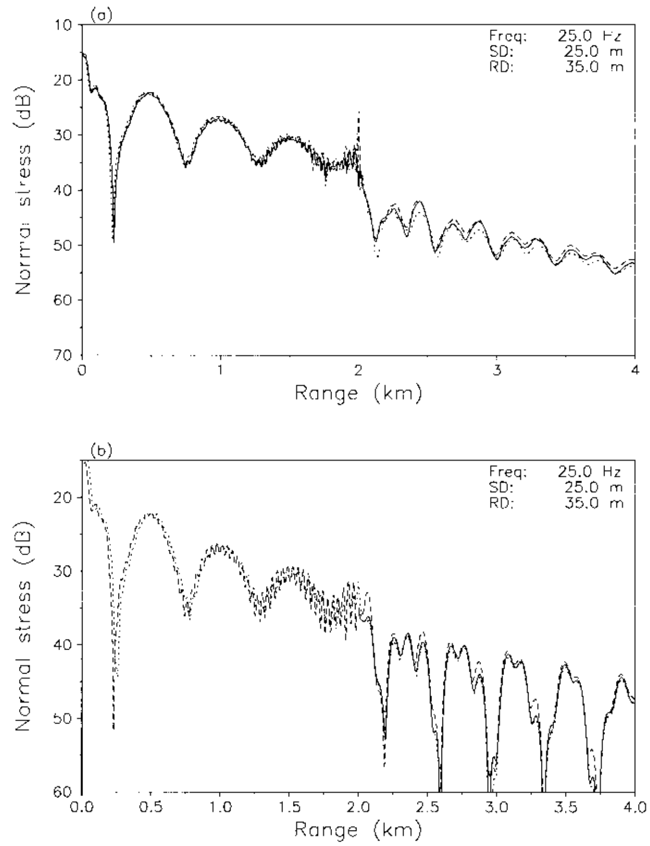

FIG. 5. Solutions to the single layer benchmarks. (a) case B3, (b) B4, solid: BEM, dashed : VISA, dotted: spectral super-element.

We first multiply both sides of Eq. (26) by $P_{m-1}(\overline{z})$. Integrating over the layer thickness and using the orthogonality properties of Legendre polynomials,

$$\int_0^{t_\ell} P_{m-1}(\overline{z})P_{k-1}(\overline{z})dz=\begin{cases}\dfrac{t_\ell}{2m-1}, & m=k,\\ 0, & m\neq k,\end{cases} \tag{27}$$

together with the identity,

$$\int_0^{t_\ell} P_{m-1}(\overline{z})e^{-i\eta z}dz=t_\ell e^{-i\eta(t_\ell/2)}i^{m-1}(-1)^{m-1}\times j_{m-1}\left(\frac{t_\ell\eta}{2}\right), \tag{28}$$

and the expressions for the source spectrums derived previously, we obtain

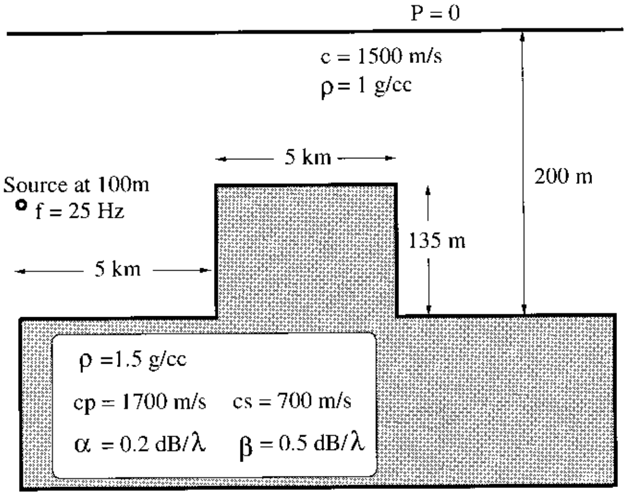

FIG. 6. Ex. C : Schematic of the elastic cylindrical seamount.

$$\hat{U}_{\ell m}(x)=C_m\sum_{k=1}^{\infty} i^{m+k-2}\int_{-\infty}^{\infty} d\eta\left\{\left[-\frac{\varphi}{\kappa^2}e^{-x\gamma}+\frac{2\eta^2}{\kappa^2}e^{-x\delta}\right]U_{\ell k}(0)+\left[-\frac{2i\eta\gamma}{\kappa^2}e^{-x\gamma}+\frac{i\eta\varphi}{\kappa^2\delta}e^{-x\delta}\right]W_{\ell k}(0)\right\}j_{m-1}\left(\frac{t_\ell\eta}{2}\right)\times j_{k-1}\left(\frac{t_\ell\eta}{2}\right), \tag{29}$$

where $C_m=(2m-1)\zeta_m t_\ell/(2\pi)$ and $\zeta_m=(-1)^{m-1}$. Expansion coefficients for the other field parameters can be obtained in a similar fashion. When evaluating these integrals, we can exploit their symmetries in (m,k) to reduce the amount of computation. In addition, for $x=0$, some of the integrals can be evaluated in closed form. In Sec. II, we discuss some of the numerical issues involved in evaluating these integrals.

4. Horizontal wave-number representations for the direct panel field

The displacement potentials in the vertical wave-number domain are

$$\begin{aligned}\phi_\ell(x,z)&=\int_{-\infty}^{\infty}\left[\frac{\varphi}{\kappa^2\gamma}\Gamma(\eta)+\frac{2i\eta}{\kappa^2}\Theta(\eta)\right]\times e^{-x\gamma}e^{-i\eta(z-t_\ell/2)}d\eta,\\ \psi_\ell(x,z)&=\int_{-\infty}^{\infty}\left[-\frac{2i\eta}{\kappa^2}\Gamma(\eta)+\frac{\varphi}{\kappa^2\delta}\Theta(\eta)\right]e^{-x\delta}e^{-i\eta(z-t_\ell/2)}d\eta,\end{aligned} \tag{30}$$

where

$$\begin{aligned}\Gamma(\eta)&=\sum_{m=1}^{\infty}U_{\ell m}(0)i^{m-1}j_{m-1}\left(\frac{t_\ell\eta}{2}\right),\\ \Theta(\eta)&=\sum_{m=1}^{\infty}W_{\ell m}(0)i^{m-1}j_{m-1}\left(\frac{t_\ell\eta}{2}\right).\end{aligned} \tag{31}$$

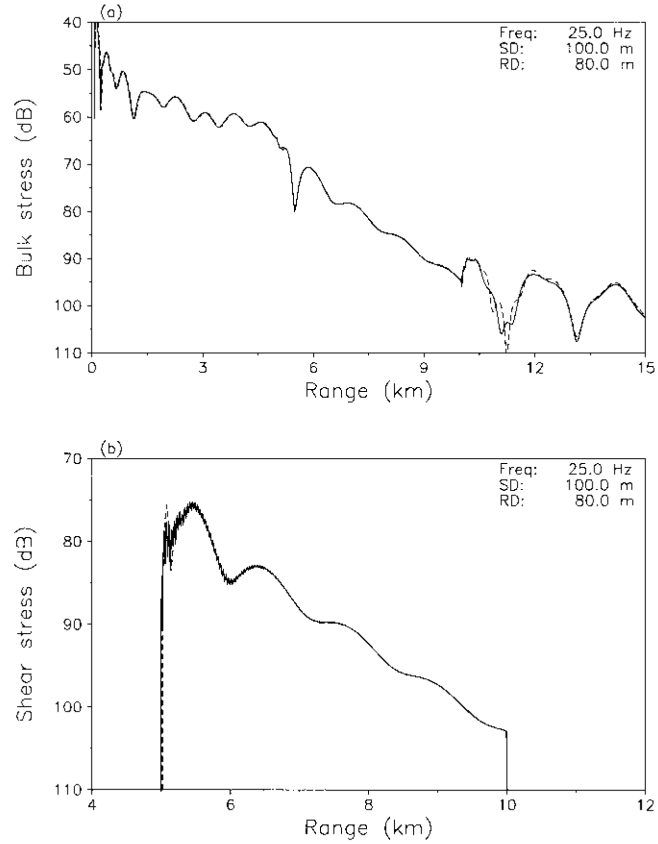

FIG. 7. Elastic cylindrical seamount (Ex. C). Receiver at 80 m. (a) Forward scattered bulk stress, (b) forward scattered shear stress. solid—VISA; dashed—spectral super-element.

The DGM method for the multi-layered sector requires the integral representations for the free-space Green's function to be expressed in terms of the horizontal wave number, s. Using contour integration as devised by Heelan,[19] the vertical wave-number integrals of Eqs. (30) are converted into horizontal wave-number integrals. After some algebra, the potentials in the s domain become

$$\begin{aligned}\phi_\ell(x,z)&=\int_{-\infty}^{\infty}\left[-\frac{\vartheta}{s\kappa^2}\Gamma(-i\mathscr{S}\alpha)+\frac{2i\mathscr{S}\alpha}{\kappa^2}\Theta\times(-i\mathscr{S}\alpha)\right]e^{-|z-\frac{t_\ell}{2}|\alpha}\frac{s}{\alpha}e^{-ixs}ds,\\ \psi_\ell(x,z)&=\int_{-\infty}^{\infty}\left[-\frac{2i\mathscr{S}\beta}{\kappa^2}\Gamma(-i\mathscr{S}\beta)-\frac{\varpi}{s\kappa^2}\Theta\times(-i\mathscr{S}\beta)\right]e^{-|z-\frac{t_\ell}{2}|\beta}\frac{s}{\beta}e^{-ixs}ds,\end{aligned} \tag{32}$$

where

$$\mathscr{S}=\mathrm{sign}(z-t_\ell/2),\quad i\alpha=\sqrt{h^2-s^2},$$

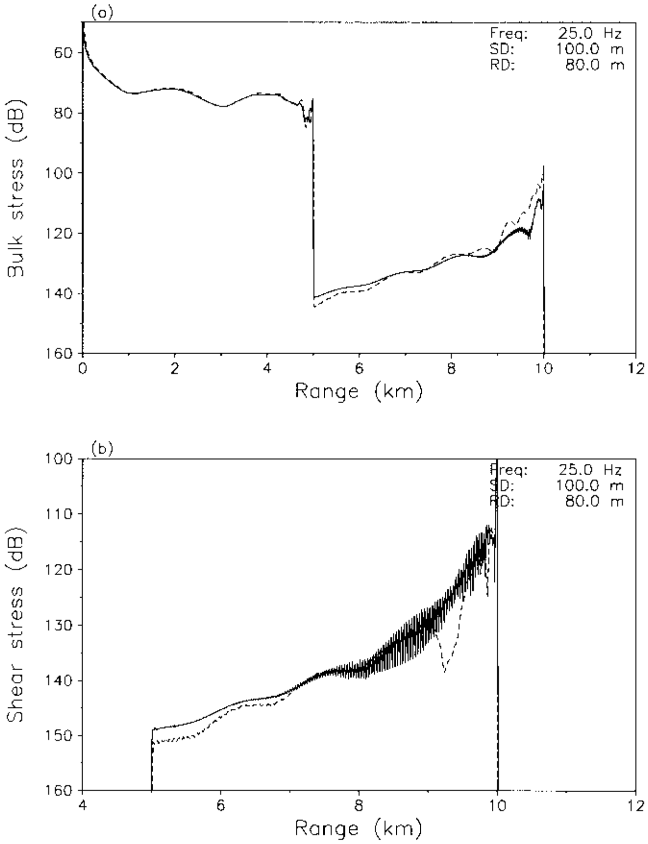

FIG. 8. Elastic cylindrical seamount (Ex. C). Receiver at 80 m. (a) Back scattered bulk stress, (b) back scattered shear stress. Solid—VISA; dashed—spectral super-element.

$$i\beta=\sqrt{\kappa^2-s^2},\quad \vartheta=2\alpha^2+\kappa^2,\quad \varpi=2s^2-\kappa^2,$$

and Γ and Θ are given by Eq. (31). The potentials given by Eq. (32) are valid only for $z\leqslant 0$ and $z\geqslant t_\ell$, but still allows for the application of the global matrix method when satisfying the horizontal interface boundary conditions since it is at the interfaces $z=0$ and $z=t_\ell$ of each layer that the fields are being matched. However, it is desirable to have a horizontal wave-number integral representation that is valid within the layer so that efficient FFP techniques can be employed for the resulting field computation. In Ref. 20 we derive a discretized equivalent point source horizontal wave-number representation for these potentials that is valid for $0\leqslant z\leqslant t_\ell$.

We now simply use Eq. (32) as the source contribution in the SAFARI code[1] to determine the associated homogeneous solution, the expansions of which are described in the next section.

D. Homogeneous solution

The horizontal wave-number integral representation for the homogeneous solution can be obtained by a direct extension of the equations presented in Schmidt and Jensen.[21] The complete homogeneous solution is given by the sum over all finite layers as well as over all orders of expansion. Using the orthogonality relation of Legendre polynomials, expansion coefficients can be extracted as

$$\overline{\mathbf{V}}_{\ell m}(x)=(2m-1)i^{m-1}\int_{-\infty}^{\infty}\sum_{n=2}^{N-1}\sum_{k=1}^{\infty}\overline{\mathbf{K}}_\ell\overline{\mathbf{E}}_\ell\overline{\mathbf{J}}_{\ell m}\times[U_{nk}(0)\overline{\mathbf{A}}_{\ell,nk}+W_{nk}(0)\overline{\mathbf{C}}_{\ell,nk}]e^{-ixs}ds, \tag{33}$$

where

$$\overline{\mathbf{V}}_{\ell m}(x)=[\overline{U_{\ell m}}\quad \overline{W_{\ell m}}\quad \overline{T_{\ell m}}\quad \overline{S_{\ell m}}]^T,$$

$$\overline{\mathbf{K}}_\ell=\begin{bmatrix}-is & -is & i\beta & -i\beta\\ -\alpha & \alpha & s & s\\ -\vartheta & -\vartheta & 2s\beta & -2s\beta\\ 2is\alpha & -2is\alpha & -i\varpi & -i\varpi\end{bmatrix},$$

$$\overline{\mathbf{E}}_\ell=\mathrm{diag}[e^{-\frac{t_\ell}{2}\alpha},e^{-\frac{t_\ell}{2}\alpha},e^{-\frac{t_\ell}{2}\beta},e^{-\frac{t_\ell}{2}\beta}],$$

$$\overline{\mathbf{A}}_{\ell,nk}=[A^-_{\ell,nk}\quad A^+_{\ell,nk}\quad B^-_{\ell,nk}\quad B^+_{\ell,nk}]^T,$$

$$\overline{\mathbf{C}}_{\ell,nk}=[C^-_{\ell,nk}\quad C^+_{\ell,nk}\quad D^-_{\ell,nk}\quad D^+_{\ell,nk}]^T,$$

$$\overline{\mathbf{J}}_{\ell m}=\mathrm{diag}\left[j_{m-1}\left(\frac{it_\ell\alpha}{2}\right),\zeta_m j_{m-1}\left(\frac{it_\ell\alpha}{2}\right),\; j_{m-1}\left(\frac{it_\ell\beta}{2}\right),\zeta_m j_{m-1}\left(\frac{it_\ell\beta}{2}\right)\right].$$

Each combination of indices n and k represents a single SAFARI run. Here $A^{\mp}_{\ell,nk}$ and $B^{\mp}_{\ell,nk}$ are respectively the up/down going compressional and shear waves in layer ℓ due to the kth order *symmetric* source in layer n. The corresponding quantities from the *antisymmetric* source are $C^{\mp}_{\ell,nk}$ and $D^{\mp}_{\ell,nk}$. However, the DGM can treat multiple right-hand sides simultaneously and hence all the amplitudes of the up/down going waves can be found with just a single global matrix inversion. This makes the algorithm very efficient even for problems with a large number of layers and high orders of expansion.

E. Element connectivity

Inserting the field expansions in Eq. (10) into the weak form of the boundary conditions in Eq. (9) leads to the *connectivity* equations between super-elements j and $j+1$. The number of equations for each layer depends on the number of expansion terms used as well as the type of media in super-elements j and $j+1$. In general, the connectivity equations are

$$\begin{Bmatrix}U_{\ell m}(x_j)\\ W_{\ell m}(x_j)\\ T_{\ell m}(x_j)\\ S_{\ell m}(x_j)\end{Bmatrix}^j=\begin{Bmatrix}U_{\ell m}(x_j)\\ W_{\ell m}(x_j)\\ T_{\ell m}(x_j)\\ S_{\ell m}(x_j)\end{Bmatrix}^{j+1},\qquad \ell=1,\ldots,N,\quad m=1,\ldots,\quad M. \tag{34}$$

Here N is the number of layers and M is the number of expansion terms used within each layer. By systematically matching boundary conditions along the vertical cut, we obtain a linear system of equations for the unknown *panel source strengths* for super-elements j and $j+1$. Once the unknown source strengths are determined, the resulting field can then be determined efficiently with DGM using the horizontal wave-number spectral representations. The reader is referred to Schmidt *et al.*[14] for a discussion on implementing an efficient marching algorithm from the system of connectivity equations.

II. NUMERICAL IMPLEMENTATION

The numerical implementation of the spectral super-element method requires careful treatment of the infinite integrals associated with the expansion coefficients of the field parameters. It is clear from Eq. (29) that at large wave numbers, the integrand is highly oscillatory with an irregular frequency determined by the relative orders of the spherical Bessel functions. In addition, at large wave numbers, we require proper cancellation of the contributions arising from the symmetric and antisymmetric sources in order to arrive at a finite value for the expansion coefficient. The matter is further aggravated by the slow decay of the integrands.

To evaluate these integrals, we use adaptive integration routines from the QUADPACK[22] library. In addition, we have implemented a brute force method in which partial sums of the integrand are first obtained by integrating in between the zeros of the oscillating integrand. An acceleration technique is then used to speed up the convergence of the partial sums. Finally, we also employ a modification of the standard Gauss–Chebyshev quadrature developed by Perez-Jorda *et al.*[23] and Perez-Jorda and San-Fabian.[24] Their formulation is particularly suited for automatic quadrature. The reader is referred to Ref. 20 for more details about the various quadrature schemes.

III. NUMERICAL EXAMPLES

In the following we illustrate how the present approach provides accurate solutions to canonical propagation and reverberation benchmark problems. We compare our solutions with results obtained from the boundary element code by Gerstoft and Schmidt,[25] the virtual source algorithm (VISA) by Schmidt[26] and the finite element parabolic equation model (FEPES) of Collins.[12] Unless otherwise noted, the super-element solutions are obtained using only four orders of expansion in the field parameters within each layer. In addition, in each of the examples, we take the water column to be lossless with a sound speed of 1500 m/s and a density of 1 g/cm^3.

A. Modified NORDA benchmark

Example A is based on case 3A used in the NORDA Parabolic Equation Workshop.[27] This problem was first modified for use as a test case for elastic PE by Wetton and Brooke[10] and we run a slightly different version here. The waveguide, illustrated in Fig. 2(a), consists of a water layer with a thickness of 100 m, over a solid layer with a thickness of 100 m, a density of 1.2 g/cm^3, a compressional speed of 1590 m/s, and a shear speed of 500 m/s. The solid has a compressional attenuation of 0.2 dB/λ and a shear attenuation of 0.5 dB/λ. A 25-Hz line source is placed at a distance of 5 km from an artificial transparent interface. The primary test here is to see how well energy is coupled through a transparent vertical interface and represents the extreme case of a low-contrast vertical step. Comparisons between SAFARI and our solutions for receiver depths of 50 and 110 m are shown in Fig. 2(b) and (c). For clarity we have shown the solution from 2 to 8 km and we see that the super-element solution agrees well with SAFARI. For ranges less than 5 km, the super-element formulation reduces to SAFARI exactly and we see perfect agreement in the solutions. For ranges beyond the artificial interface, the agreement is still quite good for both receivers, indicating proper coupling across the interface.

B. Single layer benchmarks

The next benchmark consists of a set of two-sector problems shown in Fig. 3. The waveguide is bounded at the top and bottom by a pressure release boundary. A 25-Hz line source is placed at a depth of 25 m and at a distance of 2 km from the vertical discontinuity. By bounding the waveguide by pressure release boundaries, this benchmark requires the propagation code to properly conserve energy before one can arrive at the correct answer. In addition, by varying the material properties on both sides of the discontinuity, we can assess the sensitivity of a particular code to contrast in the primary direction of propagation. Table I shows the four different configurations that we have chosen.

The BEM code[25] is expected to produce good results for this set of benchmarks and is therefore taken as the reference solution. Solutions for the normal stress σ_{zz} at a receiver depth of 35 m are shown in Figs. 4 and 5 and we generally have good agreement among the three solutions.

C. Elastic cylindrical seamount

Example C, shown in Fig. 6, consider an elastic seamount in a cylindrically symmetric ocean environment. The fluid version of this problem first appeared in Gilbert and Evans.[28] A 25-Hz source is located in the middle of the waveguide. The depth of the water column at the source range is 200 m. A 135-m-high seamount has inner radius 5 km and outer radius 10 km. The bottom is a homogeneous half-space with a compressional sound speed of 1700 m/s and a shear speed of 700 m/s. The density is 1.5 g/cm^3 and the compressional and shear attenuation in the bottom is 0.2 and 0.5 dB/λ respectively. We solved this problem using only three range sectors and eight layers down to a depth of 400 m. We show both forward and backscattered dilatational and shear stress at a receiver depth of 80 m. Comparisons between the virtual source algorithm and the super-element method are shown in Figs. 7 and 8. In forward scatter, we have excellent agreement between the two solutions.

There is also good agreement in the backscatter solutions. The increase in backscatter energy at the source range in Fig. 8(a) is due to the fact that for a point source in a cylindrically symmetric waveguide the backscattered energy focuses at the source range. The high-frequency oscillations seen in the backscatter VISA solution are due to numerical noise creeping into the *extremely* low field values computed.

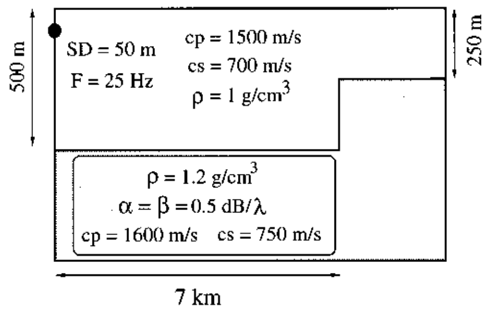

FIG. 9. Ex. D : Embedded step discontinuity.

D. Embedded step discontinuity

Example D, taken from Collins[11] and shown in Fig. 9 involves two solid layers and a step discontinuity in layer thickness. A 25-Hz source is placed at a depth of 50 m in the upper layer, which is 500 m thick for ranges less than 7 km and 250 m for ranges beyond 7 km. The compressional and shear speeds in the upper layer is 1500 and 700 m/s, respectively and the medium is assumed to be lossless. The lower layer is a half-space with compressional and shear speeds equal to 1600 nd 750 m/s, respectively. The attenuations in the lower medium is 0.5 dB/λ for both wave types. The density in the upper and lower medium is 1 and 1.2 g/cm^3, respectively. This particular problem has a very low contrast

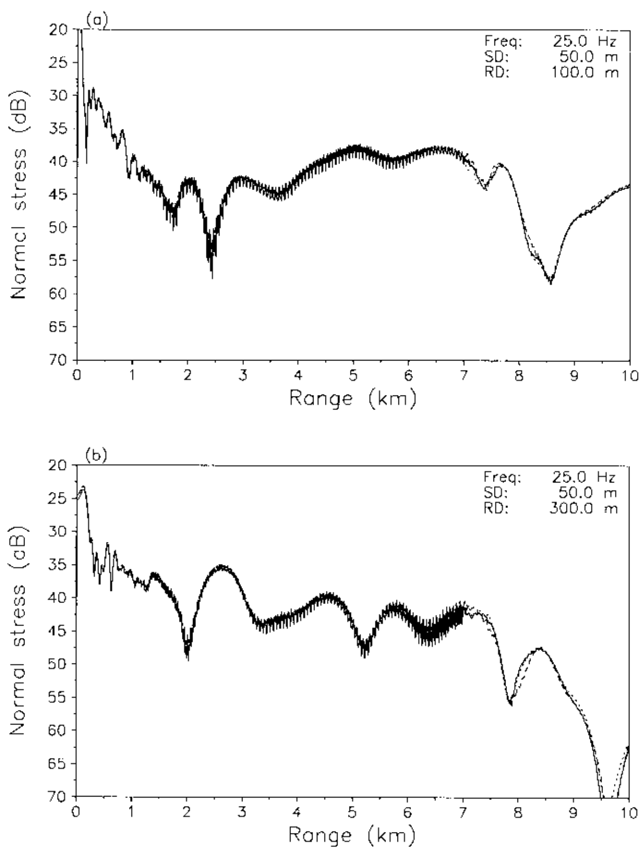

FIG. 10. Embedded elastic step (Ex. D). Total normal stress. (a) Receiver at 100 m. (b) Receiver at 300 m. Solid—BEM; dashed—VISA; dotted—spectral super-element.

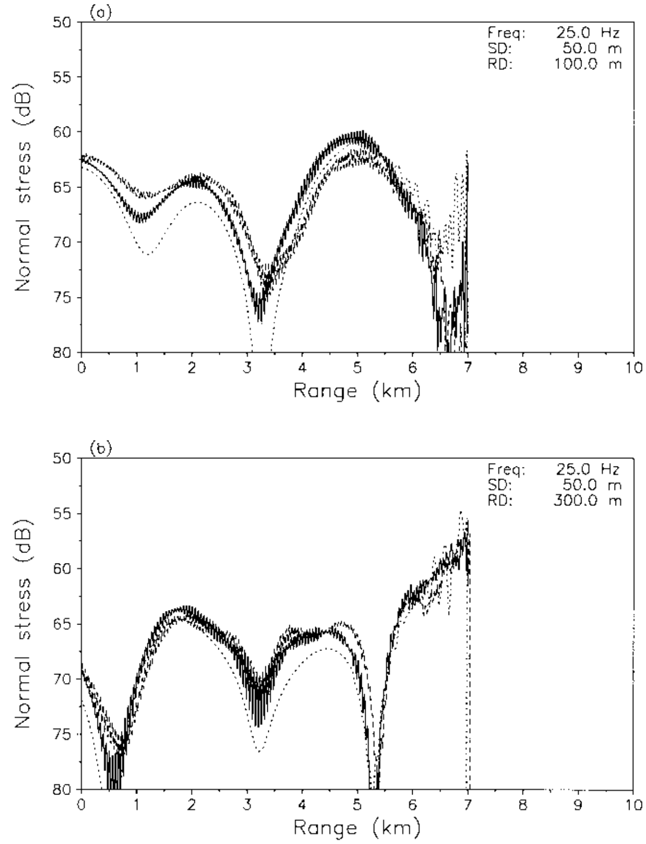

FIG. 11. Embedded elastic step (Ex. D). Back scattered normal stress solution. (a) Receiver at 100 m. (b) Receiver at 300 m. Solid—BEM; dashed—VISA; dotted—spectral super-element.

across the vertical interface and we present forward and backscatter solutions at two receiver depths. In the forward direction (Fig. 10), we have good agreement between the three solutions.

In the backscatter (Fig. 11), there is some disagreement, particularly near the scattering surface. We believed this is due to inaccuracies associated with the large dynamic range between the forward and backscattered field.

E. Elastic ASA wedge

Example E, shown in Fig. 12 is test case 3 from the Parabolic Equation Workshop II.[29] This is an elastic version of the standard ASA wedge benchmark problem. A 25-Hz point source is placed at 100-m depth. The ocean depth de-

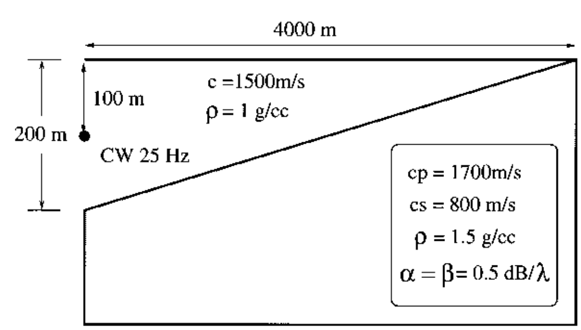

FIG. 12. Ex. E : Environment for ASA elastic wedge.

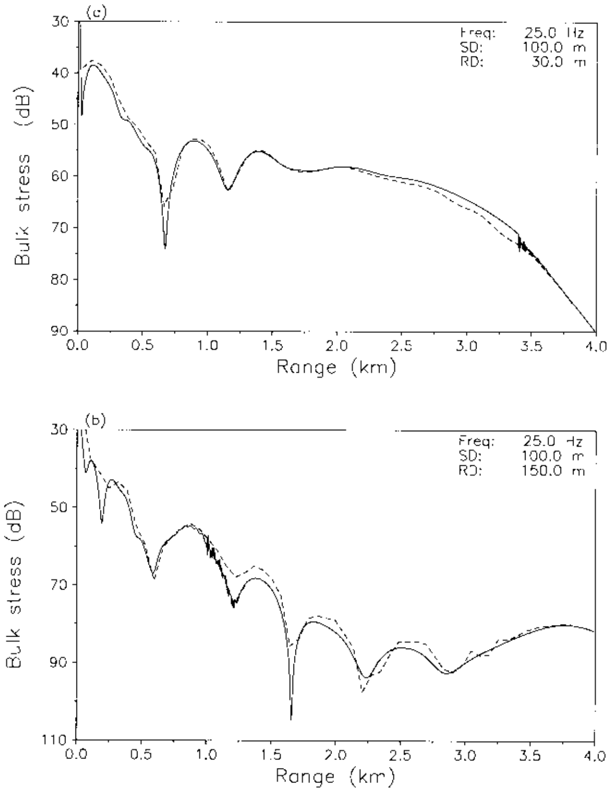

FIG. 13. ASA elastic wedge (Ex. E). (a) Receiver at 30 m, (b) Receiver at 150 m; solid—FEPE, dashed—spectral super-element.

creases linearly with range from 200 m at the source range to zero at $r=4$ km. The ocean bottom has a compressional sound speed of 1700 m/s and a shear speed of 800 m/s. The density is 1.5 g/cm^3 with the compressional and shear attenuations at 0.5 dB/λ. The environment is discretized into 17 layers, each of about a wavelength in depth, and 56 range sectors. In Fig. 13 we present solutions from the parabolic equation model and the super-element method. There is good agreement for the shallow receiver and for the receiver in the bottom, the agreement is still quite good and the differences are primarily due to the particular manner in which the environment is being discretized.

F. Step periodic roughness patch

Example F considers a step periodic roughness patch shown in Fig. 14. A similar fluid example was first treated by Evans and Gilbert.[30] The patch extends from 5–10 km and the depth variations consists of steps which are 10 m high, 100 m long and 200 m apart. Hence there are 5 steps per kilometer. The source, at a frequency of 50 Hz, is at a depth of 18 m, and Fig. 15 shows the bulk stress for receiver depths of 50 and 150 m. The spectral element solution is computed using eight orders of expansion. The transmission loss is compared to the reference solution for a flat-bottom waveguide (SAFARI). For the bottom receiver, we see an increase in the field below the roughness patch and this is a result of energy being dumped from the water column into

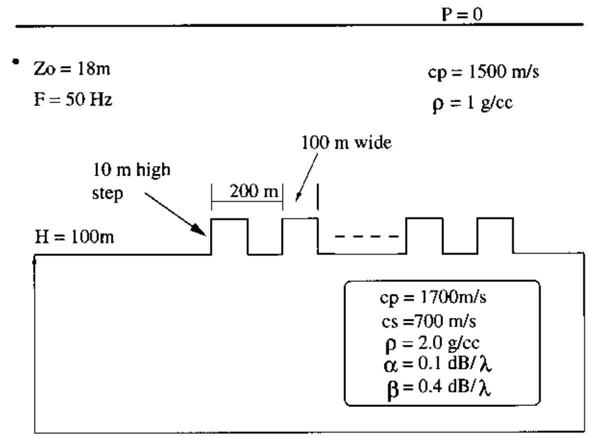

FIG. 14. Ex. F : Schematic of the periodic roughness patch.

the bottom. This behavior is most clearly seen in the contour plots of Fig. 16. This test problem provides a good example of energy loss due to bottom roughness.

IV. CONCLUSION

We have extended an earlier published super-element approach for wave propagation in multi-layered range-dependent fluid environments to handle arbitrary fluid-elastic stratifications. The approach is capable of computing both the forward scattered and the reverberant field, particularly

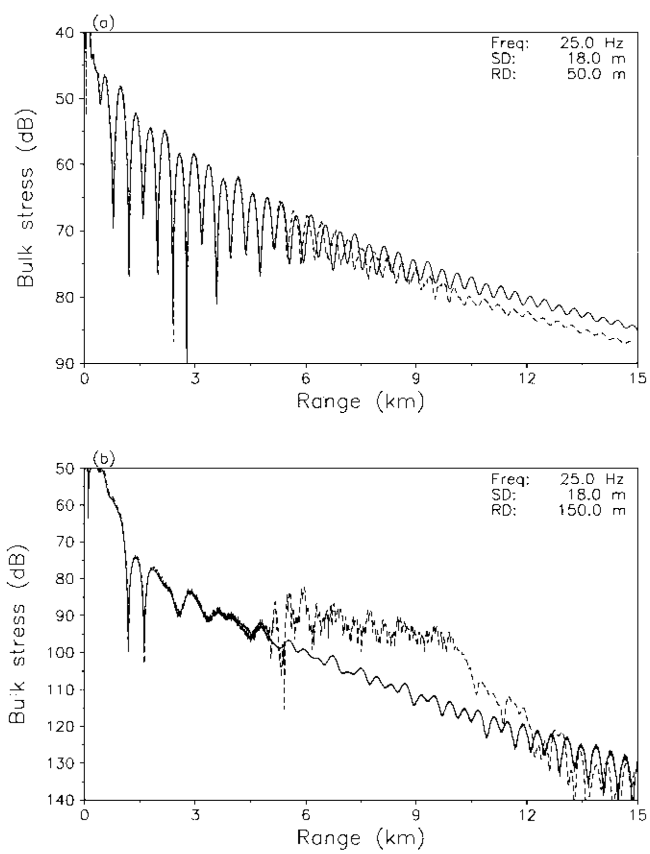

FIG. 15. Step periodic roughness patch (Ex. F). Forward dilatation : (a) Receiver at 50 m. (b) Receiver at 150 m. Solid—SAFARI; dashed—spectral super-element.

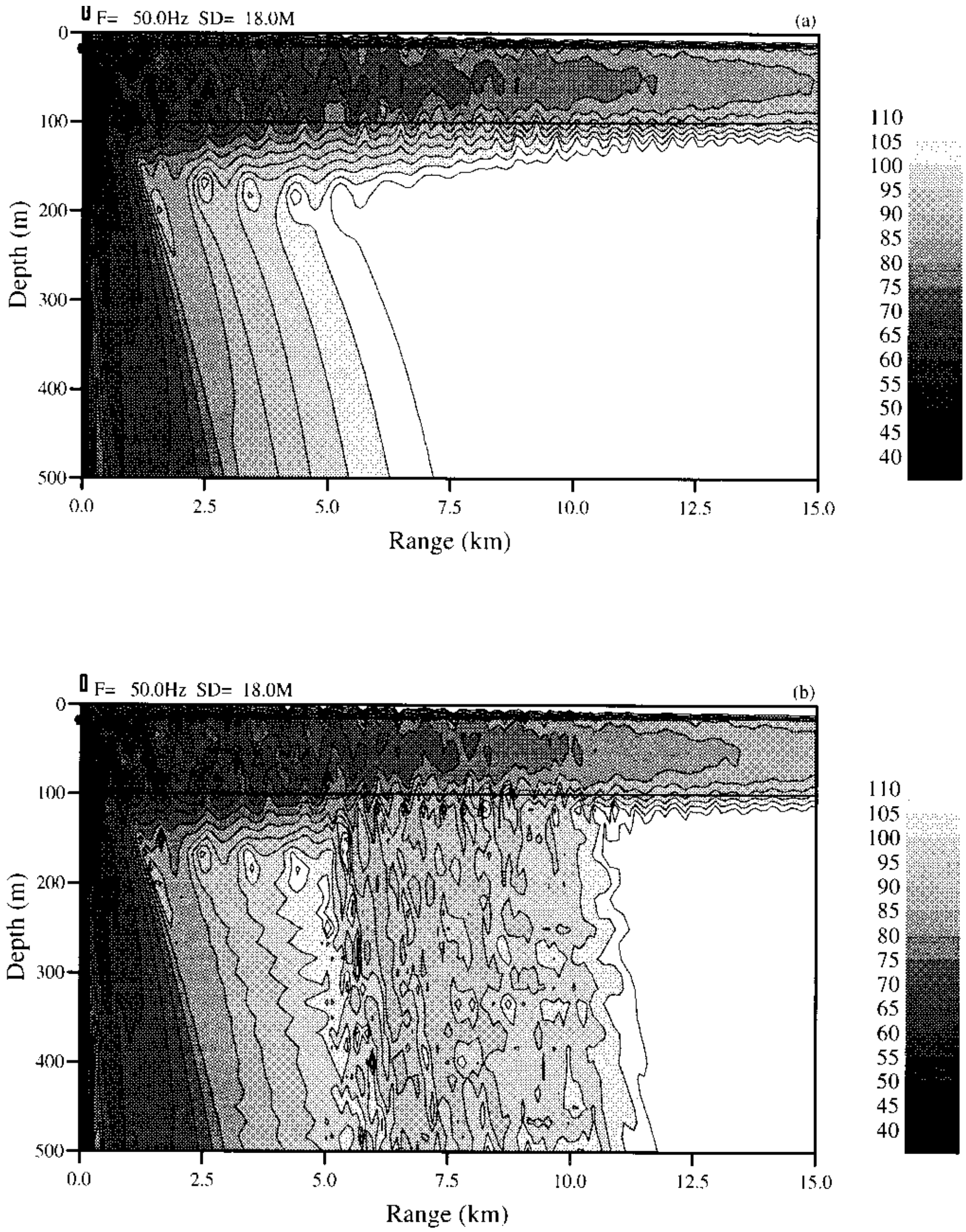

FIG. 16. Step periodic roughness patch (Ex. F). Forward dilatation : (a) SAFARI solution without the patch, (b) spectral super-element solution with the roughness patch.

suitable for treating reverberation from large scale oceanic features and canonical benchmark problems. The numerical efficiency of the approach is obtained by using SAFARI to compute all influence functions for each super-element with one global matrix inversion. Wave-number integration is also used for evaluating the field within each super-element once the boundary panel source strengths are found. Even though the extension is straightforward conceptually, its numerical implementation is nontrivial. In particular, the expansion coefficients are represented by infinite integrals that are slowly convergent as well as exhibiting rapid irregular oscillations at infinity. However, extensive numerical computations have demonstrated the performance of the present implementation, particularly in the forward scatter direction.

ACKNOWLEDGMENTS

The authors are grateful to Dr. Peter Gerstoft of the SACLANT Undersea Research Centre for useful discussions and for providing the latest version of the boundary element code. We would also like to acknowledge helpful discussions with Dr. Mike Collins of Naval Research Laboratory. This work was partially supported by the Office of Naval Research, in part by the High Latitude Dynamics and the Ocean Acoustics programs.

[1] H. Schmidt, *SAFARI: Seismo-acoustic Fast Field Algorithm for Range Independent Environments. User's Guide. SR 113* (SACLANT ASW Research Centre, La Spezia, Italy, 1987).

[2] I. T. Lu and L. B. Felsen, ''Adiabatic transforms for spectral analysis and

synthesis of weakly range-dependent shallow ocean Green's functions,'' J. Acoust. Soc. Am. **81**, 897–911 (1987).
[3] J. T. Goh and H. Schmidt, ''Validity of spectral theories for weakly range-dependent ocean environments—Numerical results,'' J. Acoust. Soc. Am. **95**, 727–732 (1994).
[4] R. A. Stephen, ''A review of finite-difference methods for seismo-acoustic problems at the sea floor,'' Rev. Geophys. **26**, 445–458 (1988).
[5] J. E. Murphy and S. A. Chin-Bing, ''A seismo-acoustic finite element model for underwater acoustic propagation,'' in *Shear Waves in Marine Sediments*, edited by J. M. Hovem, M. D. Richardson, and R. D. Stoll (Kluwer, Dordrecht, 1991).
[6] J. A. Hudson, ''A parabolic approximation for elastic waves,'' Wave Motion **2**, 207–214 (1980).
[7] J. P. Corones, B. DeFacio, and R. J. Krueger, ''Parabolic approximations to the time-independent elastic wave equation,'' J. Math. Phys. **23**, 577–586 (1982).
[8] S. C. Wales and J. J. McCoy, ''A comparison of parabolic wave theories for linearly elastic solids,'' Wave Motion **5**, 99–113 (1983).
[9] R. R. Greene, ''A high-angle one-way wave equation for seismic wave propagation along rough and sloping interfaces,'' J. Acoust. Soc. Am. **77**, 1991–1998 (1985).
[10] B. T. R. Wetton and G. H. Brooke, ''One-way wave equations for seismoacoustic propagation in elastic waveguides,'' J. Acoust. Soc. Am. **87**, 624–632 (1990).
[11] M. D. Collins, ''A two-way parabolic equation method for elastic media,'' J. Acoust. Soc. Am. **93**, 1815–1825 (1993).
[12] M. D. Collins, ''An energy conserving parabolic equation for elastic media,'' J. Acoust. Soc. Am. **94**, 975–982 (1993).
[13] F. B. Jensen and H. Schmidt, ''Spectral decomposition of PE fields in a wedge-shaped ocean,'' in *Progress in Underwater Acoustics*, edited by H. M. Merklinger (Plenum, New York, 1987).
[14] H. Schmidt, W. Seong, and J. T. Goh, ''Spectral super-element approach to range-dependent ocean acoustic modeling,'' J. Acoust. Soc. Am. **98**, 465–472 (1995).
[15] K. F. Graff, *Wave Motion in Elastic Solids* (Dover, New York, 1991).
[16] A. D. Achenbach, *Wave Propagation in Elastic Solids* (North-Holland, Amsterdam, 1975).
[17] F. B. Jensen, W. A. Kuperman, M. B. Porter, and H. Schmidt, *Computational Ocean Acoustics* (American Institute of Physics, Woodbury, NY, 1993).
[18] I. S. Gradshteyn and I. M. Ryzhik, *Table of Integrals, Series and Products* (Academic, New York, 1980).
[19] P. A. Heelan, ''Radiation from a cylindrical source of finite length,'' Geophysics **18**, 685–696 (1953).
[20] J. T. Goh, ''Spectral super-element approach for wave propagation in range dependent elastic medium,'' Ph.D. thesis, Massachusetts Institute of Technology, June 1996.
[21] H. Schmidt and F. B. Jensen, ''A full wave solution for propagation in multilayered viscoelastic media with application to Gaussian beam reflection at fluid–solid interfaces,'' J. Acoust. Soc. Am. **77**, 813–825 (1985).
[22] R. Piessens *et al.*, *QUADPACK—A Subroutine Package for Automatic Integration* (Springer-Verlag, Berlin, 1983).
[23] J. M. Perez-Jorda, E. San-Fabian, and F. Moscardo, ''A simple, reliable and efficient scheme for automatic numerical integration,'' Comput. Phys. Commun. **70**, 271–284 (1992).
[24] J. M. Perez-Jorda and E. San-Fabian, ''A simple, efficient and more reliable scheme for automatic numerical integration,'' Comput. Phys. Commun. **77**, 46–56 (1993).
[25] P. Gerstoft and H. Schmidt, ''A boundary element approach to seismoacoustic facet reverberation,'' J. Acoust. Soc. Am. **89**, 1629–1642 (1991).
[26] H. Schmidt, ''Marching wave-number-integration approach to range-dependent, two-way seismoacoustic propagation modeling,'' J. Acoust. Soc. Am. **97**, 3316 (A) (1995).
[27] J. A. Davis, D. White, and R. C. Cavanaugh, *NORDA Parabolic Equation Workshop* (NORDA Tech Note 143, 1982).
[28] K. E. Gilbert and R. B. Evans, ''A Green's function method for one-way wave propagation in a range dependent ocean environment,'' in *Ocean Seismo-Acoustics*, edited by T. Akal and J. M. Berkson (Plenum, New York, 1986).
[29] S. A. Chin-Bing, D. B. King, J. A. Davis, and R. B. Evans, *PE Workshop II—Proceedings of the Second Parabolic Equation Workshop* (Naval Research Laboratory, Washington, DC, 1993).
[30] R. B. Evans and K. E. Gilbert, ''The periodic extension of stepwise coupled modes,'' J. Acoust. Soc. Am. **77**, 983–988 (1985).